Interaction between Thermoacoustic Oscillation and Vortical Motions in Turbulent Swirling Premixed Flame

Kozo Aoki, Masayasu Shimura, Yoshitsugu Naka, Mamoru Tanahashi
Department of Mechanical and Aerospace Engineering,
Tokyo Institute of Technology, Meguro-ku, Tokyo, Japan

1 Introduction

Combustion oscillations caused by thermoacoustic instabilities are critical for operations of practical gas turbine combustors. The thermoacoustic instability occurs when fluctuations of heat release rate are in phase with pressure oscillations [1]. So far, a lot of investigations of combustion oscillations have been conducted by experiments and numerical simulations. Shimura et al. [2] applied a high speed stereoscopic particle image velocimetry (PIV) to methane-air swirl stabilized premixed flame and investigated long-term oscillation characteristics induced by interactions between large-scale vortical motions and longitudinal quarter wave mode of a combustion chamber. Durox et al. [3] experimentally investigated acoustic energy balance in terms of Rayligh criterion and analyzed thermoacoustic coupling by using two types of combustors. On the other hand, Nicoud et al. [4] theoretically investigated the validity of the Rayleigh criterion and suggest a different stability criterion in terms of fluctuation energy. As for computational works, Tanaka et al. [5] conducted direct numerical simulations (DNS) of hydrogen-air turbulent swirling premixed flame and showed the importance of short-term pressure oscillation modes for flame wrinkling in the downstream region of a micro combustor. Moreover, Motheau et al. [6] applied dynamic mode decomposition (DMD) to results of large eddy simulation (LES) and investigated oscillation modes in a gas turbine combustor. Recently, Aoki et al. [7] conducted DNS of hydrogen-air swirl stabilized flame and investigated spatial oscillation characteristics of pressure and heat release rate by applying DMD to the DNS results. However, interactions between thermoacoustic oscillation and vortical motions have not been elucidated sufficiently despite their importance for thermoacoustic instability. In this study, DMD and thermoacoustic instability analysis are conducted for the DNS results to investigate thermoacoustic oscillation characteristics and mechanisms of acoustic energy transfer by vortical motions.

2 DNS of Turbulent Swirling Premixed Flame

DNS of turbulent swirling premixed flame is conducted for two swirl number cases of 0.6 and 1.2, considering detailed kinetic mechanism and temperature dependence of transport and thermal properties. The details of the DNS are shown in our previous works [5, 7]. The size of the cuboid combustor is 15 mm in the streamwise direction (L_x) with 10 mm × 10 mm cross section ($L_y \times L_z$). The number of grid points ($N_x \times N_y \times N_z$) is 769 × 513 × 513, which is determined so that flame thickness is resolved sufficiently. The shape of the inlet is concentric annulus with 0.6 mm inner and 2.5 mm outer

Correspondence to: aoki.k.aj@m.titech.ac.jp

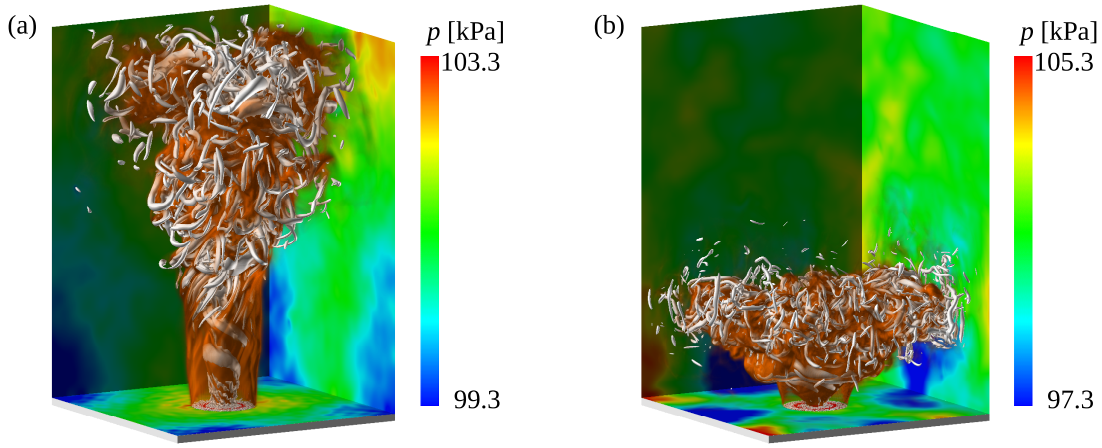

Figure 1. Pressure fluctuation on the walls, heat release rate illustrated by a volume rendering method and instantaneous contour surfaces of Q (= $0.01Q_{max}$) for S = 0.6(a) and 1.2(b).

diameters (D_{in} and D_{out}). The wall temperature is assumed to be 700 K. The equivalence ratio, pressure and preheating temperature of the unburnt premixed gas are 1.0, 0.1 MPa and 700 K, respectively. The mean axial velocity (u_{ax}) and the root-mean-square (rms) value (u'_{rms}) of velocity perturbation are 200 m/s and 13.2 m/s. In order to reproduce realistic inflow boundary conditions, the perturbations are composed of 120 sine waves with different frequencies which are every 10.59 kHz from 3.159 kHz to 1263 kHz. The phase and its lifetime of each sine wave are given by uniform random numbers. Time increment which is limited by Courant number is set to 7.5 ns in the present DNS.

Figure 1 shows pressure distributions on the walls, instantaneous contour surfaces of the second invariant (Q) of velocity gradient tensor and the distribution of heat release rate (q) illustrated by a volume rendering method. The value of the contour surfaces of Q is 1 % of its maximum value (Q_{max}). For S = 0.6, large-scale helical vortical structures are formed in the upstream region, whereas a lot of fine-scale eddies emerge in the downstream region. The distribution of heat release rate is cylindrical in the upstream region, and is complex in the downstream region since flame front is distorted by the large- and fine-scale eddies. As for S = 1.2, large-scale ring-shaped and fine-scale vortical structures can be observed in relatively upstream region and the flame structure becomes more complex than that for low swirl number case. On the other hand, pressure distributions on the walls clearly show different regular patterns for each swirl number case. It indicates that natural acoustic modes induced in the combustor strongly depend not only on the shape of the combustor but also on the swirl number.

3 Frequency Characteristics of Vortical Motions and Pressure Fluctuation

Figure 2 shows power spectra of Q at representative positions shown in our previous study [7]. These power spectra are obtained from time series data of Q during t = 337.5 μs ~ 561.0 μs at intervals of 1.5

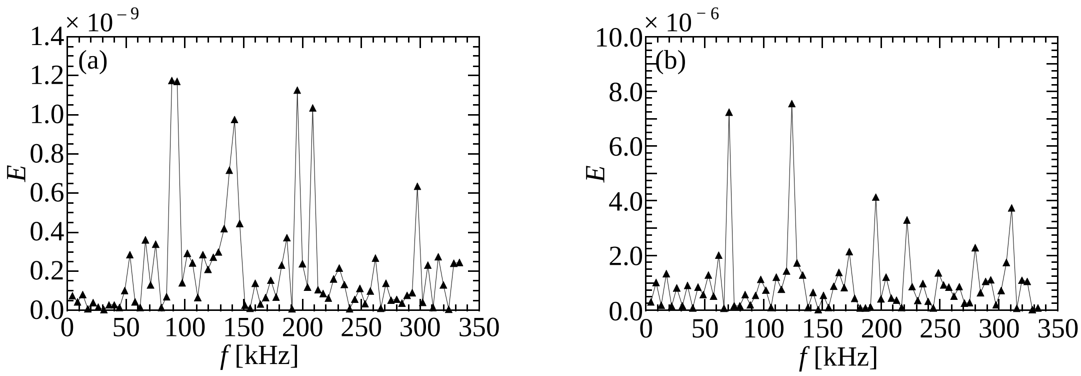

Figure 2. Power spectra of Q at representative positions for S = 0.6 (a) and 1.2 (b).

μs. As shown in Fig. 2(a), peaks are observed at 89 kHz, 142 kHz and 196 kHz. Here, large-scale ring shaped and helical shaped vortical structures, which are the representative structures for low swirl number case, are generated at about 90 kHz and 200 kHz, respectively. Therefore, the above peaks appear due to the periodic large-scale vortical motions. As for S = 1.2, peaks are located at 71 kHz,124 kHz, 196 kHz and 311 kHz. These peaks are also considered to correspond to periodic large-scale vortical motions in the inner and outer shear layers near the inlet. Moreover, it has been found that the frequencies indicating peaks in the power spectra of Q agree well with those with peaks in power spectra of pressure fluctuations at one point on a wall for both cases [7].

4 DMD Analyses of Pressure and Heat Release Rate Fields

In this study, DMD proposed by Chen et al. [8] is applied to the DNS results to investigate dominant oscillation modes of pressure and heat release rate and to extract their coherent structures. In the DMD algorithm, the relation between two consecutive time series data $\boldsymbol{x}_k$ and $\boldsymbol{x}_{k+1}$ is expressed as the following equation by using linear mapping $\boldsymbol{A}$.

$$\boldsymbol{x}_{k+1} = \boldsymbol{A}\boldsymbol{x}_k, \quad (k = 0, 1, 2, ..., m).$$

By calculating Ritz values and Ritz vectors of $\boldsymbol{A}$, the time series data can be decomposed as follows:

$$\boldsymbol{x}_k = \sum_{j=1}^{m} \lambda_j^k \boldsymbol{v}_j + \boldsymbol{r}\delta_{km}, \quad \boldsymbol{r} \perp \mathrm{span}\,(\boldsymbol{x}_0, \boldsymbol{x}_1, ..., \boldsymbol{x}_{m-1}).$$

Here, λ_j and $\boldsymbol{v}_j$ are Ritz values and Ritz vectors of $\boldsymbol{A}$. $\boldsymbol{r}$ is a residual vector and δ is the Kronecker's delta. The frequency (f_j) and growth rate (g_j) of each DMD mode are defined by $f_j = \arg(\lambda_j)/2\pi\Delta t$ and $g_j = \ln|\lambda_j|/\Delta t$, respectively. The Ritz vector $\boldsymbol{v}_j$ represents a spatial distribution of a DMD mode at f_j. In the present study, 150 samples of pressure and heat release rate in the whole domain every 1.5 μs during 337.5 μs ~ 561.0 μs are used for DMD analyses.

Figure 3 shows amplitude spectra of DMD modes of the pressure field [7]. For S = 0.6, the peak with the largest amplitude is at 14 kHz, and there are other peaks at 47 kHz, 91 kHz, 125 kHz and 197 kHz, which are indicated by arrows in Fig. 3(a). The peak at 14 kHz corresponds to the longitudinal quarter

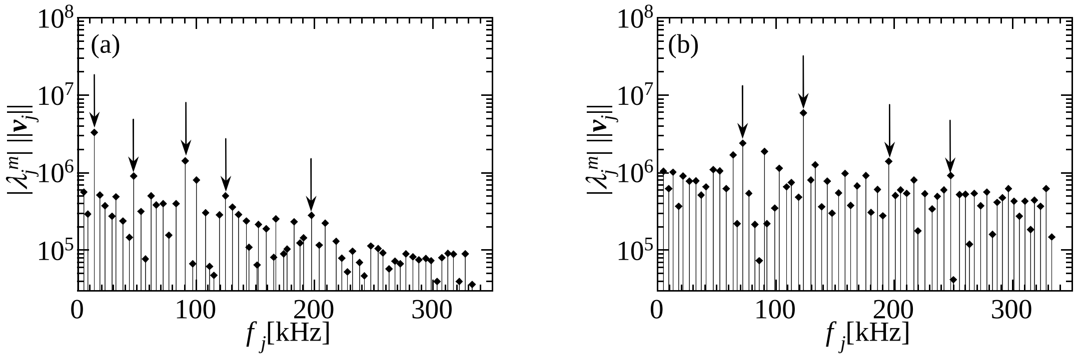

Figure 3. Amplitude spectra of DMD mode of pressure for S = 0.6(a) and 1.2(b).

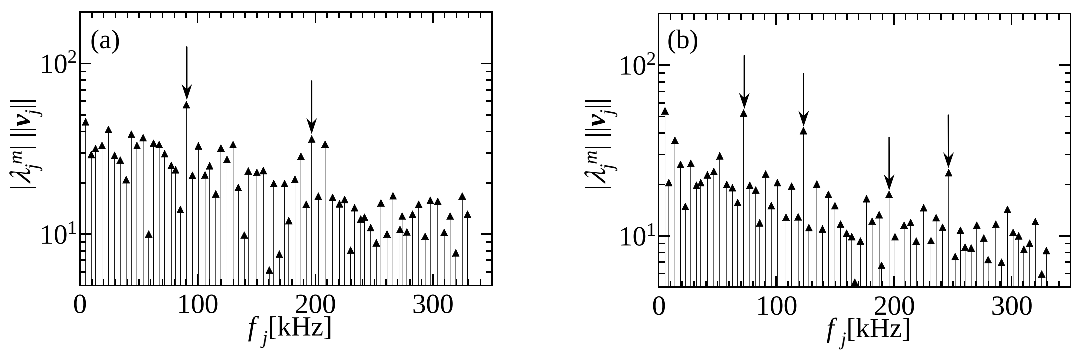

Figure 4. Amplitude spectra of DMD mode of heat release rate for S = 0.6(a) and 1.2(b).

wave mode of the combustor and the peaks at 47 kHz, 91 kHz coincide with the transverse modes. As for S = 1.2 shown in Fig. 3(b), the largest peak is observed at 124 kHz, and there are other peaks at 72 kHz, 196 kHz and 248 kHz. Thus, the peak correponding to the quarter wave mode of longitudinal acoustics cannot be observed in the spectrum for high swirl number case. This is because the growth rate of this mode (g_j) is very small. Accordingly, the quarter wave mode for S = 1.2 rapidly decays. Figure 4 shows the amplitude spectra of DMD modes of heat release rate fields [7]. For S = 0.6, the first and second peaks appear at 91 kHz and 197 kHz, respectively. As for high swirl number case, the peak with the largest amplitude can be observed at 72 kHz, and other peaks are at 123 kHz, 196 kHz and 247 kHz. From the above, there is no peak at around 14 kHz in heat release rate fields for both cases. Therefore, it is considered that heat release oscillations interact with the transverse acoustic modes rather than the longitudinal quarter wave mode. The details of the dominant DMD modes are shown in our previous work [7].

5 Thermoacoustic Instability Analysis Based on Acoustic Energy Transfer

In order to explain the reason why the above modes are dominant in the cobustor, it is necessary to elucidate the mechanism of acoustic energy transfer. As mentioned in the first section, thermoacoustic instability is induced by the coupling between oscillations of pressure and heat release rate and the product of pressre and heat release fluctuations (p’ and q’) has been considered to be one of the acoustic energy sources. In this study, DMD is also applied to the source term (p’q’) of acoustic energy equation. To capture oscillations with higher frequencies caused by the product of the fluctuations, 200 samples every 0.375 μs during 450.375 μs ~ 561.0 μs are used for the DMD analysis. By using the DMD mode $\boldsymbol{v}_j$ obtained by p’q’ data, acoustic energy $\boldsymbol{E}$ supplied during the above period T (= 110.625 μs) can be expressed as the summation of the energy $\boldsymbol{E}_j$ supplied by each mode as shown in the following equation:

$$\boldsymbol{E} = \sum_{j=1}^{m} \boldsymbol{E}_j = \sum_{j=1}^{m} \Re\left\{ \frac{1-\lambda_j^m}{1-\lambda_j} \frac{T}{m} \boldsymbol{v}_j \right\}.$$

Figure 5 shows contribution to acoustic energy transfer by each mode whose horizontal and vertical axes represent frequency and the norm of the acoustic energy $\|\boldsymbol{E}_j\|$ supplied by each mode, respectively. As shown in the Fig. 5(a), there are clear peaks at 87 kHz, 139 kHz and 203 kHz. As for S = 1.2 (Fig. 5(b)), peaks are observed at 123 kHz and 304 kHz. Thus, the frequencies where acoustic energy is actively transferred agree well with those indicating peaks in the power spectrum of Q (Fig. 2) for both cases. Therefore, it is considered that large-scale vortical motions deeply involve acoustic energy transfer. In order to elucidate the relationship between vortical motions and acoustic energy transfer, local acoustic energy supplied per cycle of a mode is investigated by focusing on the mode at about 90 kHz for S = 0.6 and at 123 kHz for S = 1.2, which are dominant frequencies in vortical motions, pressure and heat release rate fields. Figure 6 shows the DMD modes of pressure and heat release rate at 91 kHz for S = 0.6 [7]. These DMD modes are caused by transverse natural acoustic modes ($\Phi_{1,0,2}$ and $\Phi_{1,2,0}$) and the large-scale ring shaped vortical motions generated at about 90 kHz. Figure 7 shows

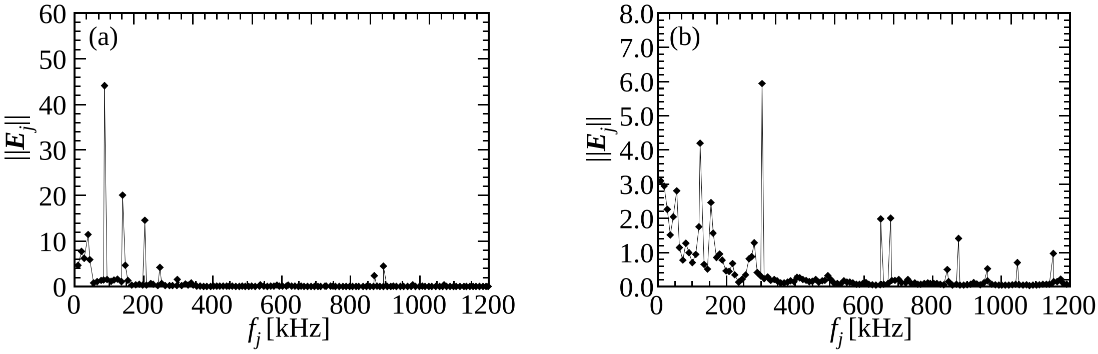

Figure 5. Contribution to acoustic energy transfer by each mode for S = 0.6(a) and 1.2(b).

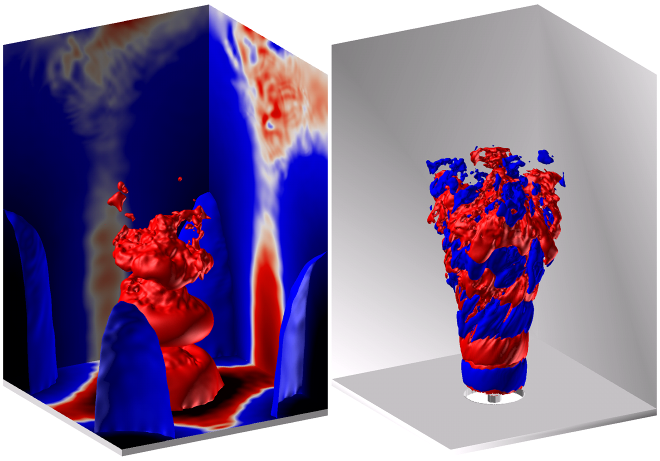

Figure 6. DMD modes of pressure (left) and heat release rate (right) at 91 kHz for S = 0.6.

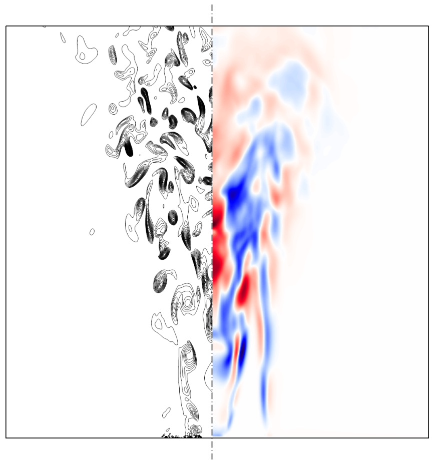

Figure 7. Instantaneous contour surfaces of Q and acoustic energy supplied per cycle of the mode at about 90 kHz for S = 0.6.

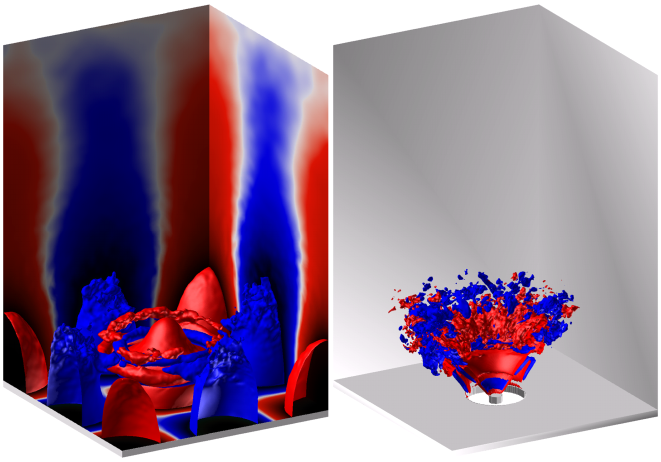

Figure 8. DMD modes of pressure (left) and heat release rate (right) at about 123 kHz for S = 1.2.

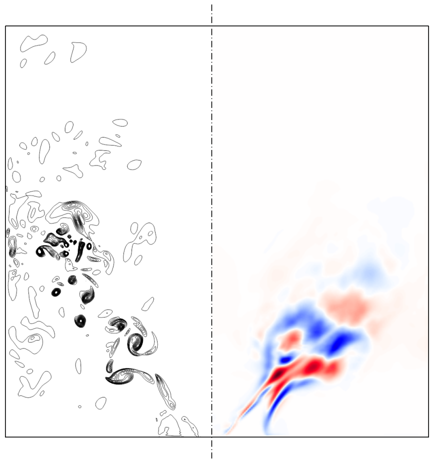

Figure 9. Instantaneous contour surfaces of Q and acoustic energy supplied per cycle of the mode at about 123 kHz for S = 1.2.

instantaneous contour lines of Q (left half) and azimuthally averaged distribution of acoustic energy (right half) in the upstream region supplied per cycle of the DMD modes of $p'q'$ at about 90 kHz for S = 0.6. In the right half figure, acoustic energy is supplied in red regions and is taken away in blue regions per cycle. From these figures, it is found that the red regions are distributed in relatively downstream region where large-scale ring shaped vortices generated in the upstream region break down and a lot of fine-scale eddies emerge. As for the DMD modes of pressure and heat release rate at 123 kHz for S = 1.2 in Fig. 8 [7], they are caused by several acoustic modes ($\Phi_{1,2,2}$, $\Phi_{4,0,2}$ and $\Phi_{4,2,0}$) and large-scale vortices generated at 124 kHz. Figure 9 shows that red regions exist in the inner and outer shear layers where large-scale ring shaped vortices are generated. Thus, the periodic large-scale vortical motions play an important role in acoustic energy supply and the acoustic modes with frequencies corresponding to those of vortex generation are induced and continue to oscillate.

6 Conclusions

In this study, DMD is applied to the DNS results of hydrogen-air turbulent swirling premixed flame for two swirl number cases and thermoacoustic instability analysis is conducted by using DMD. The DMD results of pressure fields reveal that dominant modes for S = 0.6 are not only the longitudinal quarter wave mode, but also transverse acoustic modes induced by large-scale vortical motions. As for

S = 1.2, the quarter wave mode is not a dominant mode and much shorter-term mode caused by large-scale vortical motions is most dominant. On the other hand, the DMD results of heat release rate fields show that oscillations of heat release rate interact mainly with transverse acoustic modes for both cases. The thermoacoustic instability analysis reveals that large-scale vortical motions in the upstream region and fine-scale eddies generated in the downstream region play an important role in acoustic energy supply in the combustor. These results suggest the exsitence of interactions between transverse acoustics, heat release rate and vortical motions in practical gas turbine combustors.

References

[1] Rayleigh J. (1945). The Theory of Sound. Dover (ISBN 0-486-60293-1).

[2] Shimura M, Tanahashi M, Choi GM, Miyauchi T. (2009). Large-scale vortical motion and pressure fluctuation in noise-controlled, swirl stabilized combustor. J. Therm. Sic. Tech. 4: 494.

[3] Durox D, Schuller T, Noiray N, Birbaud AL, Candel S. (2009). Rayleigh criterion and acoustic energy balance in unconfined self-sustained oscillating flames. Combust. Flame 156: 106.

[4] Nicoud F, Poinsot T. (2005). Thermoacoustic instabilities: Should the Rayleigh criterion be extended to include entropy changes?. Combust. Flame 142: 153.

[5] Tanaka S, Shimura M, Fukushima N, Tanahashi M, Miyauchi T. (2011). DNS of turbulent swirling premixed flame in a micro gas turbine combustor. Proc. Combust. Inst. 33: 3293.

[6] Motheau E, Nicoud F, Poinsot T. (2014). Mixed acoustic–entropy combustion instabilities in gas turbines. J. Fluid. Mech. 749: 542.

[7] Aoki K, Shimura M, Ogawa S, Fukushima N, Naka Y, Nada Y, Tanahashi M, Miyauchi M. (2015). Short- and long-term dynamic modes of turbulent swirling premixed flame in a cuboid combustor. Proc. Combust. Inst. 35: 3209.

[8] Chen K, Tu J, Rowley C. (2011). Variants of dynamic mode decomposition: connections between koopman and fourier analyses. J. Nonlinear. Sci. 22: 887.